A New Electronic Technique for Real-Time Correction of Heading and DC-Shift Noises in Airborne Magnetic Data

K.G. Abdel-Kader
South Cairo Electricity Distribution Co.
Ministry of Electricity and Renewable Energy
Cairo, Egypt

A.S.S. El-Kabbani

A.Yahya
Department of Electrical Engineering
Faculty of Eng., Al-Azhar University
Cairo, Egypt

F.A.S. Soliman

A.A.M. Ismail

A.M. Abdel-Maksood
Exploration Sector, Nuclear Materials Authority
Ministry of Electricity and Renewable Energy
Cairo, Egypt

Abstract— **Recent developments in airborne magnetic detection systems have made it possible to detect small Ferro metallic objects such as unexploded ordnance and land mines. However, airborne magnetic data can be really large and, therefore, there is an increasing need for a fully automatic technique that could be used to correct, in real time, the noises arise during magnetic data accusation. This paper proposes a novel electronic hardware system that implemented, tested, and applied on real survey data, where it is proved to be satisfactory for accurate removal of both the heading and dc-shift noises in acquired airborne magnetic data. These errors are severe due to dominating the airborne magnetic data in all geophysical systems applications. Finally, the proposed simple technique was proved to ideally suit for incorporation into airborne magnetic instrumentation systems.**

Keywords— Airborne magnetic; unexploded ordnance; heading; dc-shift; noise; microcontrollers.

I. INTRODUCTION

Aeromagnetic surveys are widely used to aid in the production of geological maps and are also commonly used during mineral and petroleum explorations. Some mineral deposits are associated with an increase or decrease in the abundance of magnetic minerals, and occasionally the sought after commodity may itself be magnetic (e.g. iron ore deposits), but often the elucidation of the subsurface structure of the upper crust is the most valuable contribution of the aeromagnetic data.

Aeromagnetic surveys were performed in World War II to detect submarines using a Magnetic Anomaly Detector attached to an aircraft. Also, such surveys are used to perform reconnaissance mapping of unexploded ordnance (UXO). In this concern, the main systems on board the Egyptian geophysical aircraft are magnetic, gamma ray spectrometry and gravity, which measure different physical properties of the earth [1-5]. In the case of the magnetic system, which is the point of interest within the present paper, the instrument measures the strength of the magnetic field of the earth, which provides information on the different rock types under the ground (in general the more iron in the rock the greater the magnetic field strength). It also allows geologists and the geophysicists to identify different structures in the earth. Such faults or fractures are often pathways where water, mineralized fluids (to form mineral deposits) or radon travel through the earth.

II. AIRBORNE MAGNETIC SURVEY OF EGYPT

The Nuclear Materials Authority (NMA) geophysical survey aircraft (Fig. 1.) is a twin-engine Beechcraft king Air B200SE equipped with the state-of the-art airborne geo-physical system, as well, a complete navigational and data flight recovery system. This comprises a high resolution Cesium magnetometer. Communication instruments installed on the aircraft are Collins products (Fig. 2.).

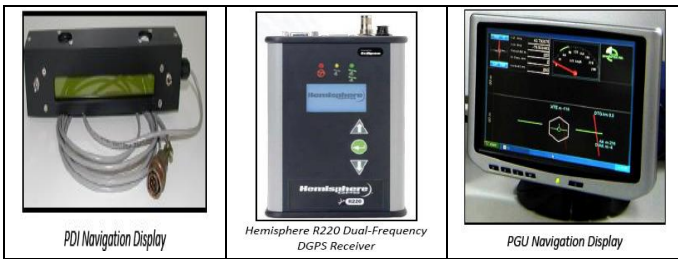Fig. 1. *Geophysical survey aircraft of Nuclear Materials Authority of Egypt.*

Fig. 2. *Airborne Navigation System.*

The Multi Sensor Magnetometer (MMS-4) is an intelligent high sensitivity, high resolution magnetometer processor. It is upgradeable to manage and process as many as four cesium magnetometers such as the CS-3 (Fig. 3). It contains a continuous frequency processing input module with a signal decouples and power control circuitry [6-10]. The MMS-4 was originally designed as a key component of Pico Envirotec's Airborne Geophysical Information System (AGIS). The processor contains synchronization input from GPS; 1.0 pps (pulse per second), to assure precise signal sampling without quantizing errors. Magnetic compensation may be undertaken in real-time on as many as three CS-3 magnetometers, simultaneously. However, if more than three CS-3 magnetometers are used simultaneously then the compensation must be undertaken as a post-mission exercise, in either case using Pico Envirotec's PEI-Comp module. [11-15].
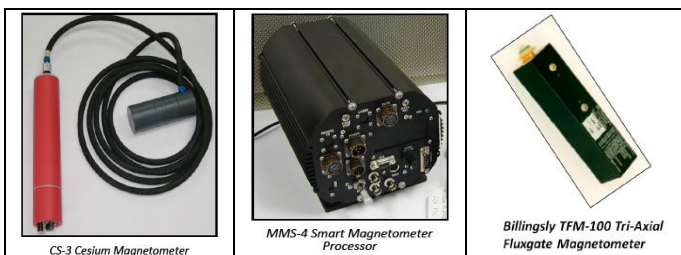

Fig. 3. *Airborne Cesium magnetometer, MMS/Cs-3.*

III. SOURCES OF DISTORTION/NOISE ON THE AIRBORNE MAGNETIC DATA

The airborne magnetic data suffers different types of noises, which in turn affects the collected data quality. Hereinafter a brief description of such noises will be described [16, 17]:

1. Air Conditioning Noise: Air condition system irregularly operates to cope with the sharp changes in the temperature of the plane during the geophysical survey, specially, over arid areas.
2. Parallax/Lag Effect: A lag effect appears due to the time takes for the sensor to move to the position of the aircraft, which is a function of the aircraft speed and the distance between the aircraft and the sensor, is known as the lag.
3. DC Shift Noise: This type of noise signature is, also, appears irregularly, the matter is due to the operation of the aircraft moving parts such as motors, ventilators, navigation systems, etc. Such

noise appears to be severe, due to the continuous air-craft movements and sudden tracking of terrain, while pilots fighting to maintain to keep constant survey altitude over the survey area.

4. Heading Effect: A heading effect causes systematic shift in the data that is a function of the direction of the travel for a survey line.
5. Figure OF merit (FOM): The aircraft should be carrying out a FOM calibration flight with all on-board systems in normal operating mode. This calibration flight was made at high altitude (10,000 feet or more) over an area of subdued magnetic gradient along the sides of a rectangular box representing the principal flying directions of the survey. The net value of the FOM should be better than 1.0 nT.

IV. DESIGN AND IMPLEMENTATION OF THE PROPOSED TECHNIQUE

A. *Design and Implementation of the Proposed Technique*

Fig. 4 shows a simplified form of the proposed system which easily implemented on EASY PIC V7.
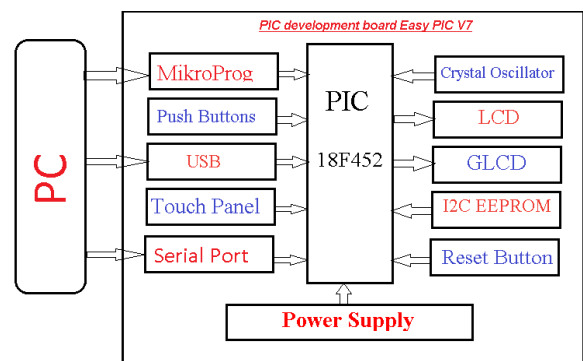

Fig. 4. *Block diagram of the proposed system implemented on Easy PICV7.*

The EasyPIC V7 is the seventh generation of the famous PIC development board. It is the product of accumulated knowledge over the past 10 years, and it is state of the art of design, functionality and quality, where board comes with PIC18F452 device. The board can be considered so unique, as it comes with powerful on-board mikroProg programmer and In-circuit debugger, capable of programming more than 250 microcontrollers (Fig.5). As well, the board has modules for all kinds of development. Beside standard DS1820 digital thermometer, LM35, analog temperature sensor was introduced. Also, Piezo buzzer was used for sound signalization and one can use 12C EEPROM to store config data. Finally, the board supports over 250 Microchip microcontrollers, and it's provided with 4-digit 7seg display, so one can build applications for LCD, GLCD and 7-Seg, all on the same board.

Fig. 5. *PIC development board "Easy PIC V7" and some of its parts used during implementation.*

V. DC- SHIFT CORRECTION TECHNIQUE

A second airborne magnetic data noise source is the dc shift. In this concern, Fig. 6 shows the DC-shift noise superimposed airborne magnetic data (Fig. 6a), true noise segment (Fig. 6b), and PIC display image (Fig. 6c). This type of noise signature is, also, appears irregularly, the matter is due to the operation of the aircraft moving parts such as motors, ventilators, navigation systems, etc. Such noise appears to be severe, due to the continuous aircraft movements and sudden tracking of terrain, while pilots fighting to maintain to keep a constant survey altitude over the survey area. So, the present part of the paper was mainly concerned with the accurate determination and correction of such noise. In this concern, the study was focused on the following steps:
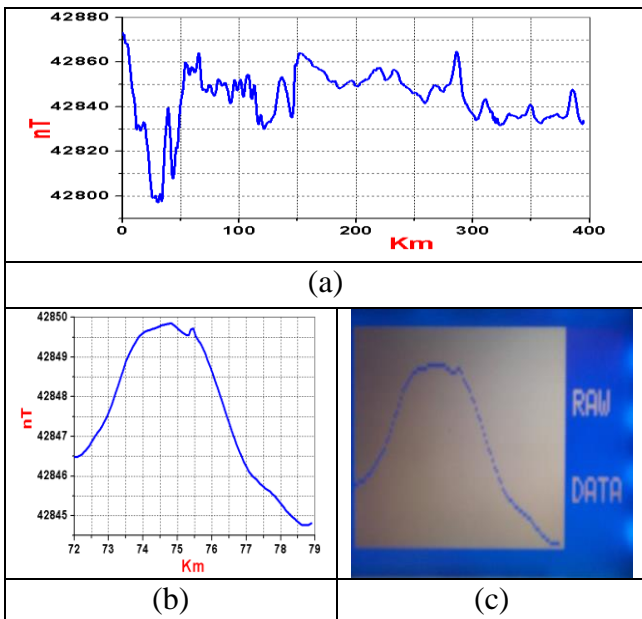

(a)

(b)   (c)

Fig. 6. *DC-shift noise superimposed airborne magnetic data (a), true noise segment (b), and PIC display image (c).*

Where: i :index number of data,
      mag :raw data,
      mag_{4diff} :data after fourth differential,
      $maxd$:value of noise dc shift,
      $index\_max$:index value of noise dc shift,
      del_dc :amount of delete noise dc shift, and
      $filter_{data}$:filter of noise dc shift data .

$$mag_{4\_diff}[n] = \sum_{n=1}^{n=p-1}(mag[n-4]-(4*mag[n+2])+mag[n-2]+(6*magp[n])+mag[n-4])/16 \quad (1)$$

$$if\ (\underset{d}{max} < mag[i])\ \{\underset{d}{max} = mag[i];\ index_{max} = i;\}\ for\ 0 < i < n \quad (2)$$

$$if\big(mag[i] > (2*mag[i-1])\big)\ \{index\_max = i-1\}\ for\ 0 < i < n \quad (3)$$

$$del_{dc} = mag[index_{max}] - mag[index\_max+4] \quad (4)$$

$$filter_{data}[i] = mag[i] + del_{dc\{for\ 0<i<n\}} \quad (5)$$

Fig. 7 shows Pseudo code of dc-shift correction.

1. START
2. READ raw_data $mag(0 … maxd-1)$
3. Calculate fourth differential (mag_{4diff}) of raw data (mag)
4. Compare value fourth differential to get index start of noise ($index_{max}$).
5. Calculate the value of delete noise (del_{dc}).
6. Result filter data by subtract value of delete noise from raw data ($filter_{data}$).
7. STOP

Fig. 7. *Pseudo code of dc-shift correction.*

After show pseudo code, the second stage is data Processing; in this stage there are steps:
Step 1: Read data from PC
Fig. 8 will show the real code which applied on kit.

```
For(i=0; i<p; i++)
   if (Usart_Data_Ready())   mag [i] = Usart_Read();
```

Fig. 8. *Code of Read Data.*

Step 2: Show Magnetic Data on GLCD
Fig. 9 shows code of Graphic-LCD which is showing data on it.

```
for(i=0;i<(P -1);i++)  Glcd_Dot(i, mag[i], 0);
```

Fig. 9. *Code of Show Data.*

Step 3: Determination of the Noise Location

```
for(i=0; i<p; i ++)
{fourth_different [i]= (mag [i+4]-  (4*( mag[i+2] + mag
[i-2]))+ (6*  mag [i]) + mag [i -4])/16.0;  }
```

Fig. 10. *Code to Get Fourth Different of Raw Data.*

Step 4: Show fourth different data on GLCD

Fig. 11 shows the code, which applied on Graphic LCD to show filter data.

```
for(i =0; i<P; i ++) Glcd_Dot(i, fourth_different [i], 0);
```

Fig. 11. *Code to Show Fourth Different of Raw Data.*

Fig. (12) shows the Airborne magnetic data after fourth differential processing (*Fig.* 12a), true noise segment (*Fig.* 12b), and PIC display image (*Fig.* 12c).
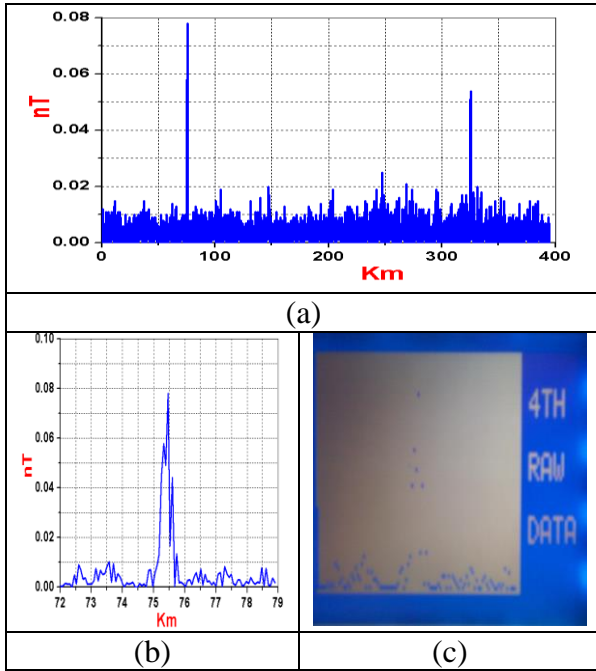
(a)

(b)

(c)

Fig. 12. *Airborne magnetic data after fourth differential processing (a), true noise segment (b), and PIC display image (c).*

Step 5: Determination of the Start Point of the Noise Signal and Noise Removal

```
for( I =4 ;  I  < P ; I++ )
{
   If ( fourth_different [I ] > 0.08 )
  {
   delete_dc_shift = mag [index] - mag [index+4];
   filter_data[I+1] =  filter_data[I +2]  =  filter_data[I +3] =  filter_data[I];
    for( j=I+4 ; j < P ; j++)
    { filter_data[j] = mag[I] + delete_dc_shift; }
  }
}
```

Fig. 13. *code Determination of the Start of Noise Signal.*

Step 6: Show Filter of Noise DC-shift Data on GLCD

```
for(I =0; I <(P -1); I ++) Glcd_Dot(I, filter_data [I], 0);
```

Fig. 14. *Show Filter of Noise Data on GLCD.*

Fig. 15 shows the net purified magnetic data obtained after removing the DC-shift noise (*Fig.* 15a), true noise segment (*Fig.*15b), and PIC display image (*Fig.* 15c).
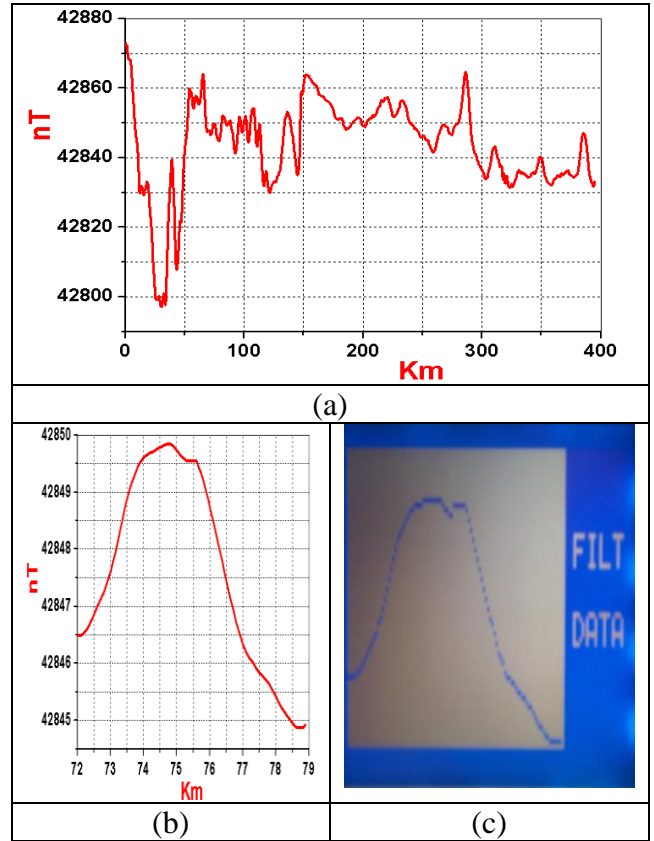

(a)

(b)

(c)

Fig. 15. *Net purified magnetic data obtained after removing the dc-shift noise (a), true noise segment (b), and PIC display image (c).*

TABLE I.   THEORETICAL AND EXPERIMENTAL DATA OF THE START VALUES OF DC SHIFT NOISE BEFORE PROCESSING.

Noise No.	Start		
	Distance (Km)	*Value Theatrical (nT)*	*Value Practical(nT)*
1	75.46	0.07819	0.08105
2	325.36	0.05419	0.05300

Step 7: Data quality Assurance

```
for(i=0; i<P; i ++)
   Filter_fourth_different[i]=(filter_data[i+4]-
(4*(filter_data[i+2] + filter_data [i-2]))+ (6*  filter_data [i])
+filter_data [i -4])/16.0;
```

Fig. 16. *Code of Data Quality Assurance.*

Step 8: Show fourth differential of Filter data on GLCD

```
for(i =0; i<P; i ++) Glcd_Dot(i, Filter_fourth_different [i], 0);
```

Fig. 17. *code Show fourth differential of Filter data on GLCD.*

Fig. 20 shows the Filter airborne magnetic data after fourth differential processing (Fig. 20a), true noise segment (Fig. 20b), and PIC display image (Fig. 20c).
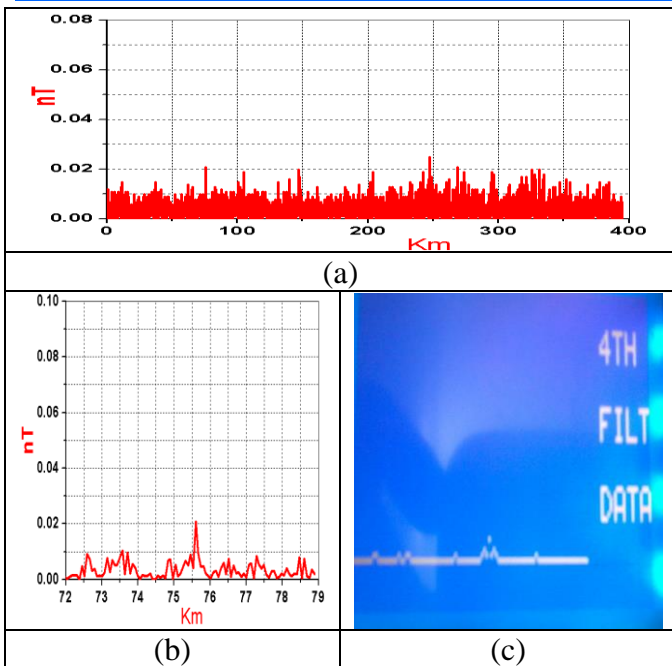
Fig. 18. *Filter airborne magnetic data after fourth differential processing (a), true noise segment (b), and PIC display image (c).*

TABLE II. THEORETICAL AND EXPERIMENTAL DATA OF THE START VALUES OF DC SHIFT NOISE AFTER PROCESSING.

Noise No.	Start		
	Distance (Km)	*Value Theatrical (nT)*	*Value Practical(nT)*
1	75.46	0.020	0.021
2	325.36	0.025	0.024

VI. HEADING CORRECTION TECHNIQUE

A heading correction process is mainly concerned with systematic shift in the data that is a function of the direction of the travel for a survey line. This is most often required in magnetic surveys because the aircraft produces a magnetic field that changes based on survey direction. Heading corrections are normally included as part of the aircraft compensation corrections that are performed automatically by the survey data acquisition system. These corrections can be determined by flying over the same point at the survey altitude in directions parallel to the planed survey lines. *Fig.* 19 shows the flight lines over a certain area, as well, the real heading flying test on four directions parallel to the planed survey lines. *Fig.s* 23 through 26 show the magnetic survey data for the predetermined flight lines number 600, 610, 10000, and 10010, respectively. In this concern, the mathematic model and its flow chart were described in the steps applied:
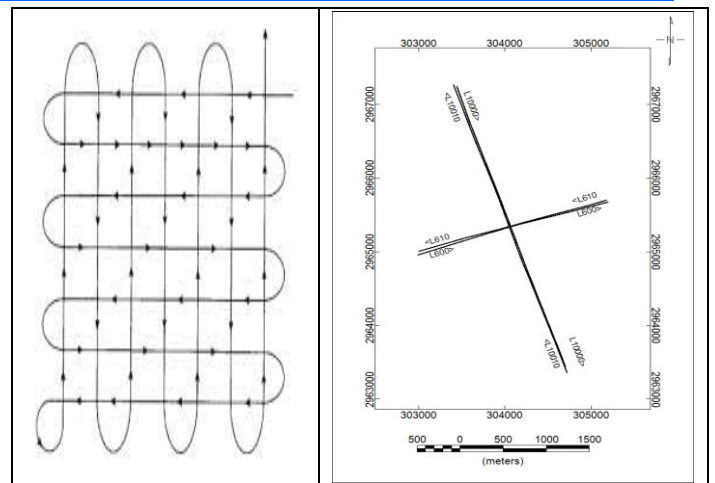

Fig. 19. *Flight lines over a certain area and heading flight lines surveying test.*

Where:
pmag1 : Magnetic data of Flight lines number 600,
pmag2 : Magnetic data of Flight lines number 610,
pmag3 : Magnetic data of Flight lines number 10000,
pmag4 : Magnetic data of Flight lines number 10010, and
max_pmag : maximum of Magnetic data of Flight lines.

$$max\_pmag1 = \frac{pmag1[i] - pmag2[i]}{2} \quad (6)$$

$$max\_pmag2 = \frac{pmag2[i] - pmag1[i]}{2} \quad (7)$$

$$max\_pmag3 = \frac{pmag3[i] - pmag4[i]}{2} \quad (8)$$

$$max\_pmag4 = \frac{pmag4[i] - pmag3[i]}{2} \quad (9)$$

Fig. 20 shows Pseudo code of the proposed heading correction procedures

1. START
2. Reading maximum number of data in the four directions (n_head_data_1 ,n_head _data_2 , n_head _data_3 ,and n_head _data_4).
3. loop iteration for reading coordinates and the value of magnetic data at each point (x, y, and Pmag).
4. Compare pmag value to get maximum value (pmax).
5. Calculate the average value of the lag between the locations of any magnetic anomaly(value_head_pmag).
6. STOP

Fig. 20. *Pseudo code of the proposed heading correction technique.*

After show pseudo code, the second stage is data Processing; in this stage there are steps:

Step 1: Read data from pc (serial port or USB)

```
For(i=0; i<p; i++)
{
    if (Usart_Data_Ready())
    {
     x1 [i] = Usart_Read();
     X2 [i] = Usart_Read();
     X3 [i] = Usart_Read();
     X4 [i] = Usart_Read();
     pmag1 [i] = Usart_Read();
     Pmag2 [i] = Usart_Read();
     Pmag3 [i] = Usart_Read();
     Pmag4 [i] = Usart_Read();
    }
}
```

Fig. 21. *Code of Read Data.*

Step 2: Show Magnetic data of Flight lines number on GLCD

```
for(i=0;i<(P -1);i++)  Glcd_Dot(i, pmag1[i], 0);
for(i=0;i<(P -1);i++)  Glcd_Dot(i, pmag2[i], 0);
for(i=0;i<(P -1);i++)  Glcd_Dot(i, pmag3[i], 0);
for(i=0;i<(P -1);i++)  Glcd_Dot(i, pmag4[i], 0);
```

Fig. 22. *Code of Show Data.*

Fig.s 23 through 26 show magnetic data of Flight lines number 600, 610, 10000, and 10010 respectively.
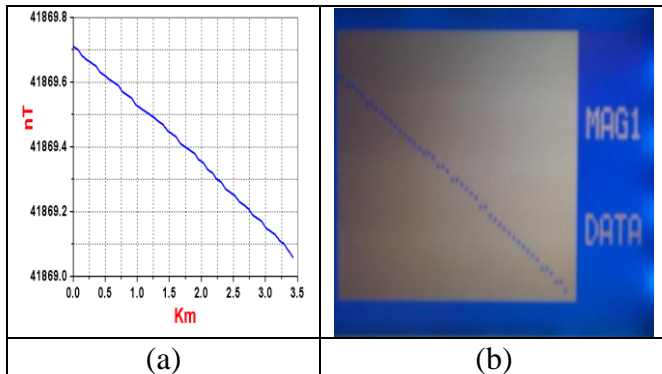

| (a) | (b) |

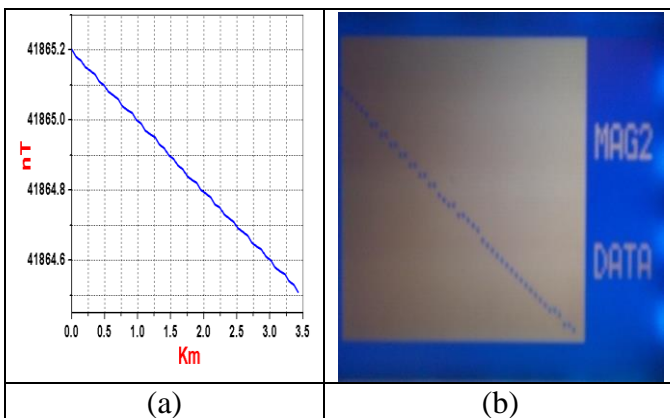Fig. 23. *Magnetic data of Flight line number 600 (a), and PIC display image (b).*

| (a) | (b) |

Fig. 24. *Magnetic data of Flight line number 610 (a) and PIC display image (b).*
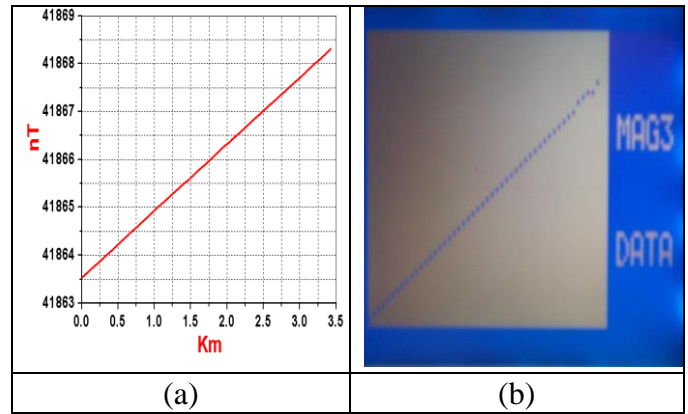

| (a) | (b) |

Fig. 25. *Magnetic data of Flight line number 10000 (a), and PIC display image (b).*
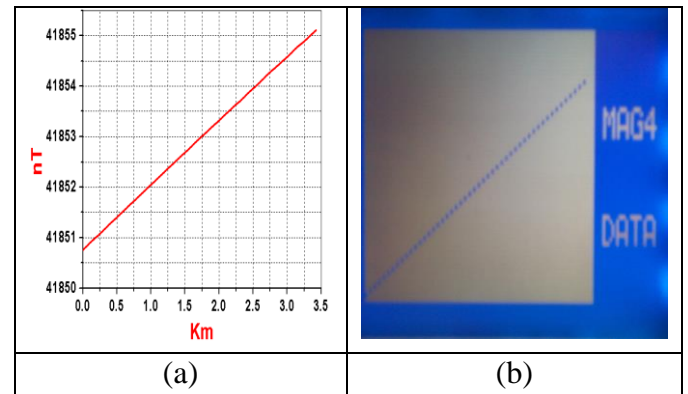

| (a) | (b) |

Fig. 26. *Magnetic data of Flight line number 10010 (a) and PIC display image (b).*

Step 3: Data Processing

```
min_sub = abs(x1[0] - x2[0]);
for(i=0;i<max_data;i++)
{   sub_x = x1[i] - x2[i];
    if(sub_x < 0.0 ) sub_x *= -1;
    if( min_sub > sub_x)
    {     min_sub = sub_x ;
        max_pmag1=(pmag1[i]-pmag2[i])/2;
        max_pmag2=(pmag2[i]-pmag1[i])/2;
       if(max_pmag1 > 0.0)
       { max_pmag1 *= -1;  max_pmag2 *= -1; }
       value_head_x1=x1  [i];
       value_head_x2=x2  [i];
       value_head_pmag1=max_pmag1;
       value_head_pmag2=max_pmag2;
    }
}
```

Fig. 27. *code of processing.*

Step 4: Show data on GLCD

```
display_float(50,2,value_head_pmag1);
display_float(50,3,value_head_pmag2);
display_float(50,6,value_head_pmag3);
display_float(50,7,value_head_pmag4);
```

Fig. 28. *code show values of heading data.*

TABLE III. THEORETICAL AND EXPERIMENTAL DATA OF THE HEADING CORRECTION VALUES.

Line	X	Y	Magnetic Data (nT)	Heading Correction theatrical (nT)	Heading Correction practical (nT)
600	304057.43	2965340.53	41869	-2.50	-2.59
610	304058.09	2965350.79	41864	+2.50	+2.59
10000	304060.29	2965352.09	41868	-4.50	-4.50
10010	304046.56	2965347.24	41859	+4.50	+4.50

Finally, Fig. 29 shows the results of the implementation.

Fig. 29. *Implementation results.*

VII. CONCLUSIONS

From the study, results, applications, and analysis of the airborne magnetic data, it is proved that the proposed simple electronic technique was highly efficient in getting rid of the both the DC-shift-and heading-noises, as well, it is ideally suit for incorporation into airborne magnetic instrumentation systems. The on board real time testing during aircraft geophysical survey for this design is our next challenge to conclude the usefulness of our proposed design applications.

REFERENCES

[1] Wikipedia,"Unexploded Ordnance", en.wikipedia.org/wiki/Unexploded Ordnance. https://en.wikipedia.org/wiki/Unexploded_ordnance

[2] M. Lambert, "Unexploded Ordnance: A Reference Guide for the Citizen", Environmental Science and Technology Briefs for Citizens, Kansas State niversitywww.engg.ksu.edu/HSRC/Tosc/uxo.pdf

[3] E. Camara, and S.Guimares "Magnetic airborne survey-geophysical flight", Geoscientfic Instrumentation Methods on and Data systems, Vol. 5, June (2016) , 181-1192.

[4] K.R.Horsfall, " Airborne Magnetic and Gamma-Ray Data Acquisition", AGSO Journalof Australian Geology and Geophysics, Vol. 17, No. 2, pp. 23-31, 1997.

[5] B. Howard, J. Aker, M. Reid "Risk Management For Unexploded Ordinance (UXO) In The Marine Environment" Vol 8, No 2 (2012).

[6] J.C. White, and D. Beamish, " The HiRES Airborne Geophysical Survey of Anglesey: Processing Report ", British Geological Survey

Environmental – Geoscience Baselines,(2010). Programme: Open Report OR/10/002.

[7] M. N. Nabighian, V. J. S. Grauch, R. O. Hansen, T. R. LaFehr, Y. Li, J. W. Peirce, J. D. Phillips, and M. E. Ruder "Geophysics Today: A Survey of the Field as the Journal Celebrates Its 75th Anniversary" Society of Exploration Geophysicists (2010) pp. 183-213.

[8] Mauring, E. and Kihle, O., "Leveling Aero-geophysical Data Using a MovingDifferential Median Filter", Geophysics, Vol. 71, pp. 5-11, (2006).

[9] Luyendyk, A.P.J., "Processing of airborne magnetic data" AGSO Journal of theAustralian Geology and Geophysics, Vol. 17, pp. 31-38, (1997).

[10] Huang,, H., 2008, Airborne geophysical data leveling based on line-to-line correlations,Geophysics, Vol. 73, pp. F83-F89, (2008).

[11] PicoEnvirotec, Inc., www.picoenvirotec.com/

[12] M. El-kattan, H. El-Henawy, Ala-Din Kamal, F.A.S. Soliman, A. Salem, and A. Osman, "Integrated detection of landmines using neutron back-scattering and magnetic gradient techniques ", 22nd Intr. Geophysical Conf. and Exhibition, Brisbane, Australia,(2012) February 26-29.

[13] M. El-Kattan, A. Salem, F.A.S. Soliman, Ala-din Kamel, Hadia El-Hennawy, "Microcontroller based neural network for landmine detection using magnetic gradient Data", 4th Intr. Conf. on Intelligent and Advanced Systems, ICIAS2012, Kuala Lumpur, Malaysia, 12-14 June (2012) , pp. 46-50.

[14] K. Davis, Y. Li and M. Nabighian "Automatic detection of UXO magnetic anomalies using extended Euler deconvolution" Vol. 75, (2010).

[15] M. Elkattan, Mohamed Elsayed "Detection of Landmines Using Innovative Technologies", Ph.D. Thesis, Faculty of Engineering, Ain-Shams University, Cairo, Egypt, (2013). Nuclear Materials Authority, P.O.Box 530, Maadi-11728, Cairo, Egypt.

[16] M.Abdel-Maksood, "Electronic Implementation of Hopfield Neural Network for Depth Determination of Buried Ferro-Metallic Objects", Ph.D. Thesis, Faculty of Engineering, Al-Azhar University, Cairo, Egypt., (2011), Nuclear Materials Authority, P.O.Box 530, Maadi-11728, Cairo, Egypt.

[17] A.S.S.El-Kabbani,K.G.Abdel-Kader, A.A.M.Ismail,   F.A.S.Soliman,   and   A.M.Abdel-Maksoud, "Design and Application of an Automatic Technique for Maneuvers Correction of airborne Magnetic Data", Egyptian Geophysical Society, EGS: Vol. 12, No. 1, January (2014), pp. 113-121.